Accepted for presentation in: 30th IEEE Int. Symposium on Local and Metropolitan Area Networks (LANMAN), Boston, USA, July 2024.

Custom Design and Experimental Evaluation of Passive Reflectors for mmWave Private Networks

Simon Häger, Marco Danger, Karsten Heimann, Yasin Gümüs, Stefan Böcker, and Christian Wietfeld
Communication Networks Institute (CNI), TU Dortmund University, 44227 Dortmund, Germany
E-mail: {Simon.Haeger, Marco.Danger, Karsten.Heimann, Yasin.Guemues, Stefan.Boecker, Christian.Wietfeld}@tu-dortmund.de

***Abstract*—Future 6G private networks rely on millimeter-wave (mmWave) cells for ultra-high local connectivity, but non-line-of-sight (NLOS) scenarios demand costly dense deployments. Instead, a new approach gaining much attention in research introduces intelligent reflecting surfaces (IRSs) to increase coverage with fewer full-blown active antennas. In an earlier work, we introduced and validated a new passive IRS architecture leveraging additive manufacturing to provide reflections tailored exactly to the needs of a specific scenario. The design goal for so-called HELIOS reflectors is to procure a geometry realizing high power gains for mobile devices in a well-defined service area. This contribution introduces a design process coupling electromagnetic (EM) simulations with differential evolution-based optimization to custom-tailor the reflector shape. Our indoor measurements confirm the specified reflection characteristics and find that up to, on average, 41.2 % higher gain in receive power is attained over a broad angular range compared with a narrow-reflecting IRS. By increasing the IRS size, the peak gain of 20 dB can be matched. Moreover, it is found that the designed HELIOS reflectors support the entire mmWave spectrum. An additional benefit is given by the fact that the sub-6 GHz anchor link attains power gains of up to 12 dB from the same reflectors.**

I. Introducing Scalable Passive Reflectors for Efficient mmWave Communications

Wireless networks increasingly operate within the mmWave spectrum to accommodate the ever-increasing traffic demands. There, hostile propagation conditions make it challenging to realize coverage in NLOS regions, as they occur in indoor factory (InF) environments. Illumination of these shadow regions by additional base stations (BSs) is deemed inefficient owing to both costs and energy consumption. Against this background, IRSs have emerged as an efficient alternative that dynamically reflects EM waves into a desired NLOS region [1], as shown in Fig. 1. Emerging prototypes underline the potential of this approach, however, integration challenges still need to be addressed in the coming years. For example, the IRS size must be scaled for sufficient gain to apply to large industrial scenarios. Moreover, control signaling and channel estimation procedures of current generation networks must evolve for compatibility [2]. These drawbacks can be avoided when using passive IRSs, that is, non-reconfigurable IRSs [3].

IRSs typically consist of synthetic unit cells that steer the reflection by introducing phase shifts, but the challenging implementation for mmWave frequencies prohibits scalability [2]. However, passive mmWave IRSs have emerged with limited configurations, e.g., [4] and [5]. By contrast, geometry-based IRSs intelligently realize the desired reflection behavior using

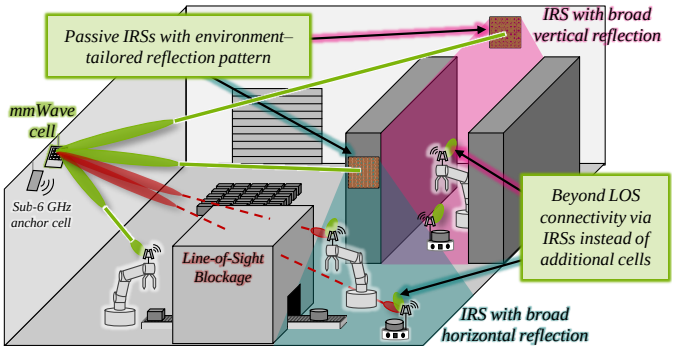

Fig. 1. Installing passive IRSs in mmWave wireless network to improve connectivity without deploying additional antennas. Each IRS is custom-tailored to exhibit the reflection characteristic determined by network planning.

a suitably dimensioned and shaped reflector geometry [6–8] that can be easily manufactured [8]. We recently proposed the *Holistic Enlightening of bLackspots with passIve reflectOr moduleS* (HELIOS) concept where large, complex geometries are realized by an array of individually parametrized modules [9], see details in Sec. II. Narrow reflections are simple to configure, as such, prior experiments successfully deployed HELIOS to extend mmWave connectivity to an user equipment (UE) in NLOS [3, 10]. Considering real-world InF scenarios, numerous requirements in terms of reflection direction, gain, and width must be fulfilled by careful selection of module parameters. This work addresses this problem by introducing a simulative design process for configuring the IRS geometry.

The remainder of this work is structured as follows. The HELIOS approach is introduced in Sec. II. Afterward, Sec. III describes the proposed EM simulation-based, genetic configuration approach that is employed to configure two HELIOS reflectors for different InF use cases. Sec. IV then characterizes the reflection behavior, including a comparison against other passive IRSs, and also assesses synergies for the sub-6 GHz anchor link. Last, Sec. V concludes with a summary.

II. Intelligent Shaping of Radio Connectivity Through Geometric HELIOS Reflectors

Mounting flat or curved metallic surfaces on walls was shown to be effective in selected deployment scenarios for frequencies up to the sub-THz spectrum, which is expected for 6G [11, 12]. However, complex mounting systems would be required in most scenarios to attain a reflection in the desired direction. Moreover, due to the expected large surface dimensions for sufficient gain, these simple reflectors would exhibit

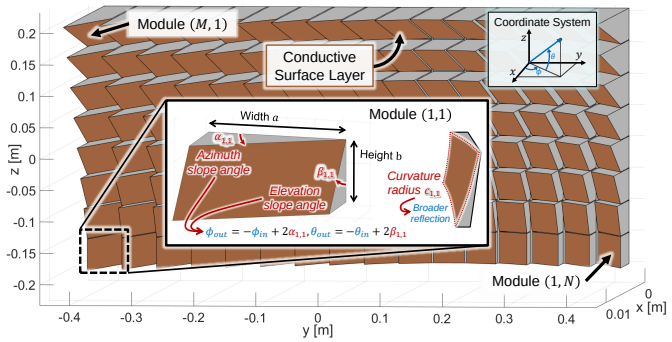

Fig. 2. Example of wall-mounted 8×16 HELIOS reflector geometry.

an undesirable protrusion [13]. Owing to this, a diffraction grating-like approach ought to be used to reduce the protrusion while maintaining the desired reflection direction [6, 7]. Employing modules with different slopes and curvatures, the radiation pattern can be customized to match the requirements set by the network operator's planning process. Additionally, self-shadowing induced power losses, which do not arise with flat IRSs [14], can be mitigated by a smart module arrangement.

This is realized by HELIOS reflectors [9] consisting of a $M \times N$ array of modules with an $a \times b$ footprint in the y-z-plane, see Fig. 2. The reflective surface orientations are set by horizontal and vertical slope angles $\alpha_{m,n}, \beta_{m,n} \in (-90°, 90°)$. The main reflection is then directed towards the angles $(\phi_{out}, \theta_{out}) = (-\phi_{in} + 2\alpha_{m,n}, -\theta_{in} + 2\beta_{m,n})$ for an incident EM wave from direction (ϕ_{in}, θ_{in}), defined by the azimuth (ϕ) and elevation (θ) angles at the IRS. Concave curvature $c_{m,n}$ imprints a sphere of equivalent radius in the $\alpha_{m,n}$-$\beta_{m,n}$-tilted reflecting surface for a broader reflection. Compensation for the aforementioned inter-module shadowing is possible employing module spacings d_y, d_z, and height offsets $h_{m,n}$.

The above-described HELIOS architecture provides the degrees of freedom to realize complex geometries that fulfill the network operator's requirements. Numerous parameters of the IRS need to be carefully set with their impact on the reflection behavior, described by the radar cross section (RCS) σ, being characterized using EM simulations [6, 9]. Hence, a brute-force design process would be infeasible for computing time reasons, instead necessitating a heuristic process, see Sec. III.

At last, the final reflector design is then 3D-printed and spray-coated with a conductive varnish, thus allowing for rapid manufacturing and deployment, as showcased in [3, 10]. In some deployment scenarios, mounting space for IRSs may be limited such that multi-functional facade elements are required. In this work, we will therefore also consider HELIOS reflectors that leverage a 3D-printed scaffold upon which transparent, reflective metamaterial foils are fastened, cf. [11]. Future use cases of this concept could be, e.g., windows or solar balcony power plants allowing light to pass into the buildings or to generate power whereas the EM waves of an outdoor wireless network are reflected as configured.

III. EM Simulation-driven IRS Design Process

This section first introduces an iterative reflector configuration process in Sec. III-A. It is subsequently used to design two HELIOS reflectors. These shall be evaluated in Sec. IV using the indoor measurement setup presented in Sec. III-B.

A. Custom Reflection Pattern Using Differential Evolution

1) Solution Approach: In this work, we adopt a genetic algorithm (GA) which is broadly adopted in the field of wireless communications owing to its capability to, with high probability, identify the global optimum for optimization problems with numerous local extrema or dependency on multiple parameters [15]. Moreover, the choice for such an algorithm is further underlined by related works, e.g., in [7] the heights of modules of a mechanic sub-THz reflectarray and in [16] the phases of a mmWave IRS's unit cells were optimized.

Similarly, we employ the differential evolution algorithm using a random initial population consisting of several chromosomes, each representing an individual HELIOS configuration. The contained genes of a chromosome represent individual parameters of the HELIOS reflector, see Sec. II for details.

- *Design Goal*: Against this background, the goal is to find the chromosome that *uniformly maximizes the reflection gain* σ (RCS, in dB) along the *target angular range of interest* Ω_{out} in ϕ_{out}-θ_{out}-domain with $\Omega_{out} \subseteq [-90°, 90°] \times [-90°, 90°]$. To promote this, we employ the *objective function*

$$\psi\left(\Omega_{out}\right) = \exp\left\{ \left|\Omega_{out}\right|^{-1} \cdot \sum_{(\phi_{out},\theta_{out}) \in \Omega_{out}} \sigma\left(\phi_{out}, \theta_{out}\right) \right\}, \quad (1)$$

since increasing low RCS values in Ω improves ψ more than improving high RCS values in the summation term. By iteratively following the subsequently discussed two phases through numerous generations, the contained chromosomes, i.e., IRS configurations, converge to the optimal solution.

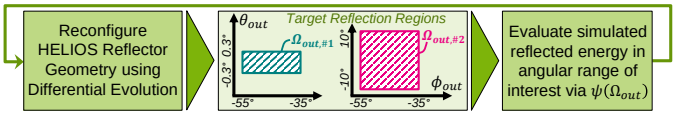

(a) Iterative reflection broadening for scenario-tailored IRS deployment.

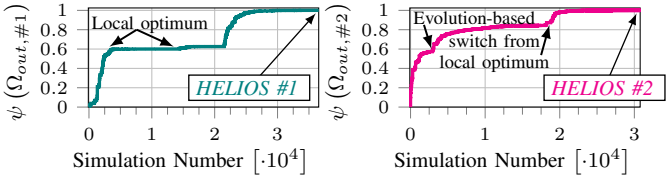

(b) Broadening hor. reflection. (c) Broadening hor. & vert. reflection.

Fig. 3. Normalized objective function ψ over time for the respective design processes. Termination after reaching plateau state.

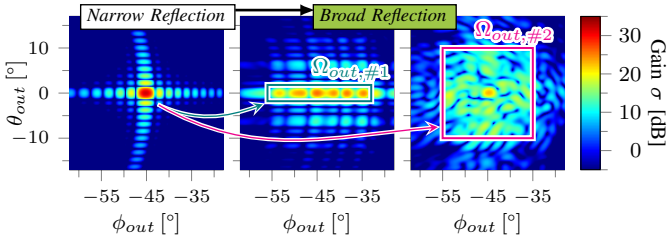

(a) Flat plate. (b) HELIOS #1. (c) HELIOS #2.

Fig. 4. EM simulation-based 28 GHz reflection patterns of designed HELIOS reflectors compared to flat reflecting surface of same size.

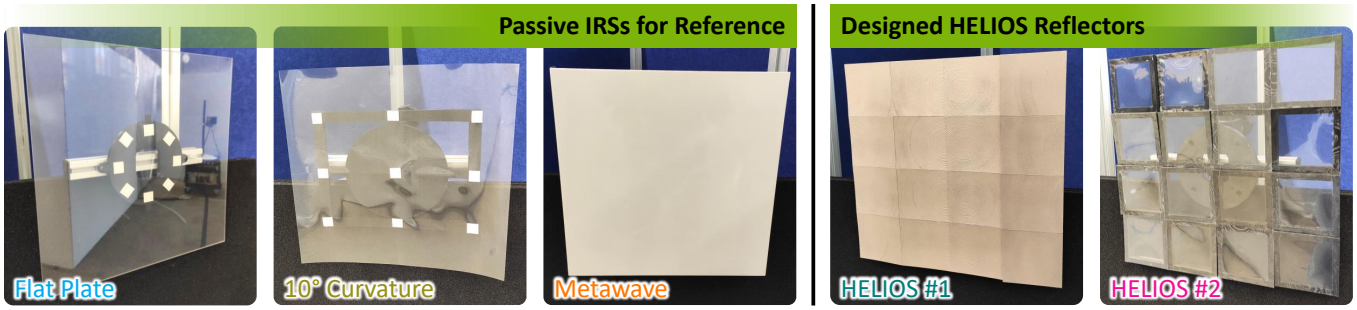

(a) Flat acrylic plate with transparent reflecting metamaterial foil by *Sekisui*. Behaves like a metal plate [11].

(b) 10°-curved metamaterial foil for a broad horizontal reflection similar to HELIOS #1 [11].

(c) Dipoles-based passive IRS by *Metawave* [4]. Configured like HELIOS #2 according to product sheet.

(d) HELIOS reflector #1: 3D-printed with conductive spray-coating. Broad horizontal reflection.

(e) HELIOS reflector #2: 3D-print is equipped with metamaterial foil patches. Broad hor. & vert. reflection.

Fig. 5. mmWave reflectors under test mounted in the indoor measurement scenario. IRSs in *(d)–(e)* are simulative designed in Sec. III-A2.

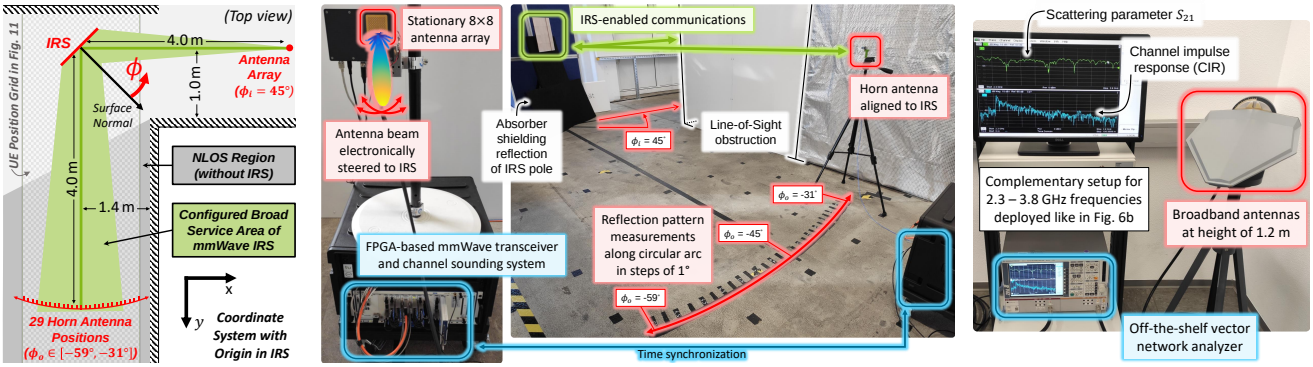

(a) Measurement scenario. (b) 28 GHz transceiver system and reflecting surface during measurements. (c) Sub-6 GHz channel sounder.

Fig. 6. Experimental evaluation scenario: Around-corner mmWave connectivity improvement of private network is realized by well-configured IRS.

- In the *selection phase*, EM simulations with *Ansys HFSS* are carried out automatically for each contained chromosome. The bistatic RCS solver then feeds the calculated reflection gains $\sigma(\Omega_{out})$ back to the optimizer, which is then used to evaluate the reflection gains along Ω_{out} using the objective function ψ. Chromosomes with high fitness are kept in the population whereas the ones with low fitness are discarded. The subsequent *recombination and mutation phase* replenishes the chromosomes by adaptive use of a suitable crossover scheme, but both crossover rate CR and mutation factor F also self-adapt throughout the runtime[1].

2) Shaping Passive IRSs with the Proposed Approach: Two HELIOS reflectors with 16 modules in a 4×4 array are configured with an overall footprint of $40\,\mathrm{cm}\times40\,\mathrm{cm}$. As the focus in our previous work was on redirecting the reflection in the desired direction [10], we instead consider reflection broadening in this work. For this reason, we use module curvatures with all $c_{m,n} = 1.0\,\mathrm{m}$, leaving 32 horizontal and vertical slope angles $(\alpha_{m,n}, \beta_{m,n})$ to be configured: The first reflector (#1) shall horizontally distribute the reflection with 20° beamwidth using $\Omega_{out,\#1} = [-55°, -35°] \times [-0.3°, 0.3°]$. The second HELIOS reflector configuration (#2) extends this by also exhibiting 20° vertical beamwidth, i.e., $\Omega_{out,\#2} = [-55°, -35°] \times [-10°, 10°]$. Whereas the angular range $\Omega_{out,\#1}$ is sampled at a resolution of 0.1°, we use 0.5° for the second reflector to reduce the prolonged EM simulation time owing to the increased size of $\Omega_{out,\#2}$ against $\Omega_{out,\#1}$. Both reflectors are designed using *Ansys HFSS* given an incident planar EM wave from $(\phi_{in}, \theta_{in}) = (45°, 0°)$ at a 28 GHz carrier in 5G band n257.

Fig. 3 depicts the respective objective function values over more than 30,000 iterations illustrating convergence to the design criteria. The resulting reflection patterns are shown in comparison to a flat plate of equal size in Fig. 4. It can be seen that the reflection has been broadened as desired, e.g., realizing a mean gain of 19.5 dB for HELIOS #1 in $\Omega_{out,\#1}$. It can be seen for HELIOS #2 that the gains in the angular regions of interest are not constant, thereby highlighting the challenge of reflecting into an approximately 40-times larger angular serving area than targeted for HELIOS #1. The two IRSs have been manufactured according to Sec. II for hands-on evaluation, see Figs. 5d and 5e. Moreover, their configurations are provided in Tab. I allowing for reproduction of this work.

TABLE I. HORIZONTAL & VERTICAL SLOPES (α, β) OF DESIGNED IRSS.

HELIOS #1

$(\alpha,\beta)_{m,n}$	$n=1$	2	3	4
$m=1$	$(-2.77°, -0.02°)$	$(+2.59°, +0.01°)$	$(-1.02°, -0.01°)$	$(+4.70°, +0.01°)$
2	$(-2.90°, -0.03°)$	$(+2.70°, +0.03°)$	$(-0.97°, -0.01°)$	$(+4.69°, +0.05°)$
3	$(-2.93°, -0.05°)$	$(+2.68°, +0.01°)$	$(-0.99°, -0.01°)$	$(+4.80°, +0.01°)$
4	$(-2.96°, -0.13°)$	$(+2.84°, +0.10°)$	$(-1.16°, -0.06°)$	$(+4.89°, +0.02°)$

HELIOS #2

$(\alpha,\beta)_{m,n}$	$n=1$	2	3	4
$m=1$	$(-0.53°, +5.05°)$	$(-0.05°, +5.45°)$	$(-0.37°, +3.56°)$	$(\ 0.00°, -2.21°)$
2	$(+4.20°, +0.29°)$	$(+4.00°, \ 0.00°)$	$(\ 0.00°, -4.80°)$	$(\ 0.00°, -5.33°)$
3	$(+0.11°, -5.84°)$	$(+0.39°, -3.68°)$	$(-1.55°, +0.00°)$	$(+2.09°, +0.22°)$
4	$(-3.93°, -0.41°)$	$(-2.98°, -0.31°)$	$(+3.17°, \ 0.00°)$	$(-2.52°, -0.22°)$

[1] Pygmo 2.19.6 documentation. Self-adaptive differential evolution algorithm. [Online]. Available: https://esa.github.io/pygmo2/algorithms.html (Accessed 2024-05-30).

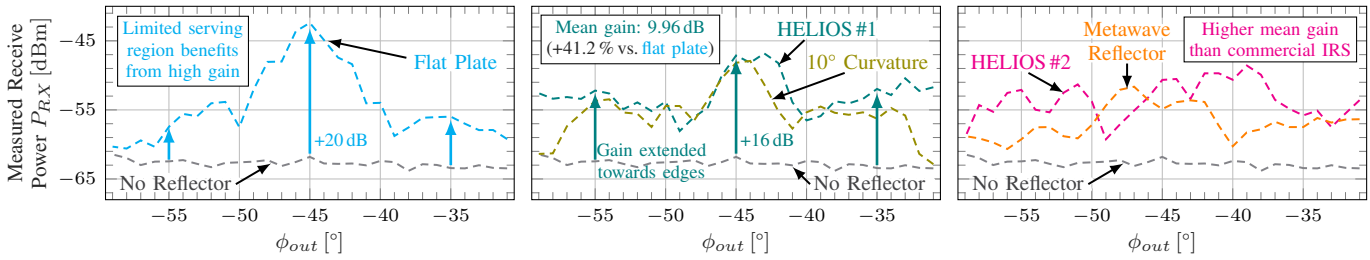

(a) Focused reflection. (b) Horizontally broadened reflection. (c) Broad reflection.

Fig. 7. Measured power with and without passive IRSs: Broad reflection of HELIOS designs is validated and similarly configured IRSs are outperformed.

B. Evaluation Scenario, Use Cases, and Methodology

In Sec. IV-A the two designed HELIOSs are evaluated and compared against other passive mmWave IRSs, as shown in Fig. 5. An InF-typical scenario is adopted, as sketched in Fig. 6a, with the goal to broadly extend connectivity around a corner. The reflection pattern towards UEs is acquired by receive power P_{RX} measurements along a circular path with a radius of 4 m in steps of 1° and aggregated over at least two sweeps. Fig. 6b depicts this for HELIOS #1 employing a mmWave channel sounder system, which is presented in detail in our previous work [9]. This is repeated for uniformly-scaled IRSs with 70 cm instead of 40 cm side lengths.

Thereafter, Sec. IV-B characterizes the reflection behavior of the designed IRSs along different frequencies using *Ansys HFSS*, configured similarly to Sec. III-A2. First, we consider the 5G spectrum from 0.5 GHz to 71 GHz in 250 MHz steps, thus spanning frequency ranges 1 and 2 (FR1, FR2). As FR2 cells are accompanied by an FR1 anchor cell, this study is deepened by channel path loss $S_{2,1}$ measurements, cf. Fig. 6c.

Last, Sec. IV-C assesses the attained beyond line-of-sight (LOS) mmWave connectivity on a larger scale using the *Wireless InSite* ray-tracer integrating the reflection pattern from *Ansys HFSS* as in [3]. The InF use cases of the designed IRSs, as sketched in Figs. 1 and 11, are considered one after the other: First, we consider the horizontal reflection by HELIOS #1 serving automated guided vehicles (AGVs), that transport goods between machines and storage, in the $8.0\,\mathrm{m} \times 2.8\,\mathrm{m}$ UE grid with 2.5 cm resolution at height of 1.2 m (like IRS and BS). Second, we study the broad reflection impact of HELIOS #2 for UEs within a logistic storage rack system. The connectivity is assessed by path loss empirical cumulative distribution functions (ECDFs) incorporating the above-described UE grid at heights from the ground up to 3 m in steps of 10 cm.

IV. Performance Evaluation of Passive IRSs

This section is split into two parts. First, the designed HELIOS reflectors are evaluated at 28 GHz in Sec. IV-A. Subsequently, the impact on the anchor sub-6 GHz link is studied in Sec. IV-B. Last, Sec. IV-C concludes with an assessment of the attained connectivity level throughout the indoor scenario.

A. Comparing Reflection Characteristics of Customized IRSs

Starting with the reflection of the flat reflecting surface in Fig. 7a, the receive power increases by up to 20 dB against the baseline value of, on average, −62.8 dBm without IRS. This corresponds well with the measurements in a similar setup in [17]. The measured reflection pattern matches simulation results in Fig. 4a although there is an offset of about 10.0 dB which arises as the boosted propagation path was not dominant beforehand with a path power of about −73 dBm, cf. Fig. 11a.

When instead mounting HELIOS #1, see Fig. 7b, the reflection is broadened such that more power can be observed for UEs on the edge of the arc, i.e., $\phi_{out} \leq -55°$ and $\phi_{out} \geq -35°$. The up to 8 dB larger gains at the cost of 4 dB peak gain in the center result in an overall mean gain amounts of 10 dB against the baseline. This constitutes a 41.2 % better performance than the flat plate. Comparing this HELIOS to the curved reflector, better performance is observed due to a broader main reflection and more power off-center. In regards to HELIOS #2, a less noticeable main lobe and, overall, a lower mean gain is observed owing to the vertical reflection broadening. However, a higher receive power can be observed at most angles than for the similarly-configured Metawave IRS, thereby underlining the feasibility of the adopted approach.

The above results show that a lower maximum gain is achieved due to distributing the energy along a larger angular region. A natural countermeasure would be an increase of the IRS size which is investigated in Fig. 8 based on the example of HELIOS #1. Beginning with the measurement results for the HELIOS reflector of increased size, a broad reflection with mean gain of 13.3 dB is observed. The peak is now on par with the smaller flat metal plate. It shows that a customized HELIOS geometry may be simply uniformly scaled if more gain is desired. Beyond local network deployments, it underlines the potential of large-scale reflector installations providing high power gains in large NLOS regions.

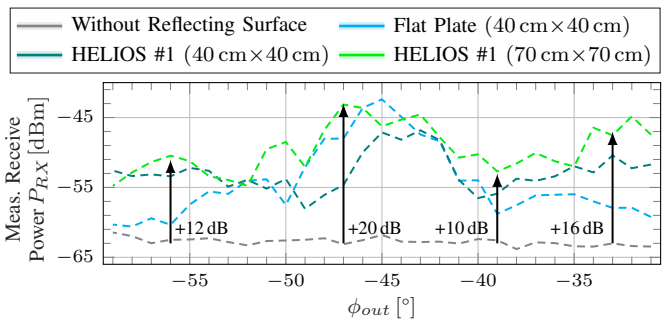

Fig. 8. Scalability analysis: Strong reflection similar to narrow-reflecting IRS is attained, but serving broad angular range with a mean gain of 13.3 dB.

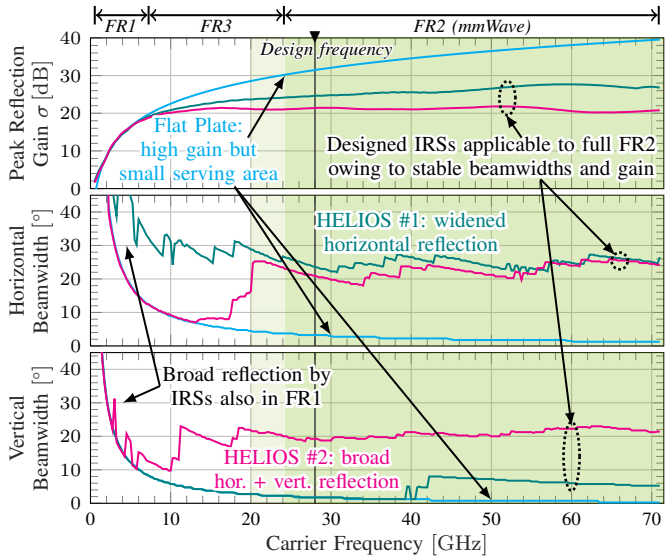

Fig. 9. Impact of carrier frequency on the reflection of the proposed IRSs.

B. Bandwidth Aspects and Impact on Anchor Link

The reflectors were designed for a carrier frequency of 28 GHz which is part of 5G band n257 which is 3 GHz broad. This raises the question of whether the reflector is applicable for the entire band or even beyond. Hence, in Fig. 9 the peak gain as well as horizontal and vertical bandwidths of the two HELIOS reflectors and a flat reflecting plate are considered.

It can be observed that the peak gain of both designed IRSs is comparably stable in FR2 compared to the steadily increasing gain for the flat plate. This is accompanied by similarly stable horizontal reflection beamwidths compared to an increasingly narrow beam for the flat reflector. The vertical 10 dB reflection width of HELIOS #2 is also stable whereas the horizontal reflection of both HELIOS #1 and the plate increasingly narrows for higher frequencies. At the lower end of the spectrum, we observe that the reflection behavior of HELIOS #2 deteriorates from the design requirements, i.e., the horizontal and vertical beamwidths become too small for frequencies below 20 GHz and 11 GHz, respectively. In contrast, HELIOS #1 remains applicable in the prospective 6G FR3 spectrum although, like for the flat plate, the gains keep decreasing for smaller carrier frequencies. Overall, Fig. 9 shows that the customized HELIOS reflectors can be used in the whole FR2 spectrum spanning tens of GHz, which marks a contrast to synthetic IRSs which have much smaller bandwidths [2].

Regarding FR1, we observe in Fig. 9 that all three reflectors behave similarly with less gain but broader reflections at increasingly lower frequencies. This can be attributed to the protrusion of the individual HELIOS modules becoming small against the wavelength, thus ensuing increasingly scattering-like behavior for lower frequencies. As noted earlier, mmWave communications is aided by anchor links in the sub-6 GHz FR1 spectrum. With high likelihood, the respective antennas are co-deployed in private networks, as shown in Fig. 1, so that the HELIOS reflector geometry might also affect the sub-6 GHz anchor link. We thus assess this by measurements for typical anchor frequencies from 2.3 GHz to 3.8 GHz using HELIOS#2 with the results being depicted in Fig. 10. There, a mean path loss of −65 dB is captured along the circular arc when no reflector is mounted. After installing HELIOS #2 or the flat plate with a footprint size of $40\,\mathrm{cm} \times 40\,\mathrm{cm}$, the path loss is reduced by about 12 dB. This gain is broadly available for UEs in the desired angular range from $\phi_{out} = -55°$ to −35°, thus validating the simulation results in Fig. 9. Scaling both reflectors to the size of $70\,\mathrm{cm} \times 70\,\mathrm{cm}$, the path loss is even reduced by up to 20 dB. This shows that geometry-defined mmWave IRSs like HELIOS are also beneficial for the anchor cell connectivity, so that the transmit power could be reduced. For the identified gains of more than 10 dB, power consumption of 5G UEs in FR1 is reduced in the order of a two-digits percentage [18], thereby increasing battery lifetime.

C. Around-corner Connectivity Extension using IRSs

Thus far, the impact of IRSs on UEs positioned on the circular arc, depicted in Fig. 6, has been assessed. Using the experimentally validated reflection patterns, this section assesses connectivity along the entire shadowed corridor like a mobile network operator would during mmWave network planning. For this purpose, we compare the radio environmental maps (REMs) before and after mounting the IRSs as mobile network operators would during network planning.

For the case where all the UEs are at the height of the IRS in Fig. 11a, it can be observed that the simulative-designed HELIOS reflector broadly improves the connectivity, whereas the narrow-reflecting IRS serves a smaller region but with a higher peak gain. Here considering mobile AGVs, the custom IRS is preferable for a robust link at all positions in the corridor. The gains by HELIOS #1 over the flat plate are approximately 15 dB at the sides of the corridor ($|x| > 0.7\,\mathrm{m}$). In the deep shadow area ($y \gg 4\,\mathrm{m}$), the customized IRSs reduce path loss even more effectively, with gains of up to about 30 dB over the baseline path loss without reflector installation. This shows that the full benefits of the customized reflectors are attained at larger distances than in the previous measurement setup.

Finally, we assess the connectivity for UEs at different heights, here for the example of robotic arms for warehouse shelves, as depicted in Fig. 11b. As it is not practical to show 3D heatmaps, we employ path loss ECDFs, which show that

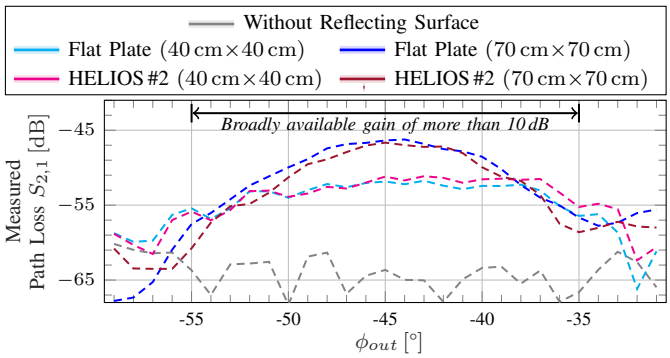

Fig. 10. Designed mmWave reflectors at sub-6 GHz anchor cell frequency: As a positive side-effect, and over a wide range of positions, shadowed UEs benefit by an improved link budget of more than 10 dB.

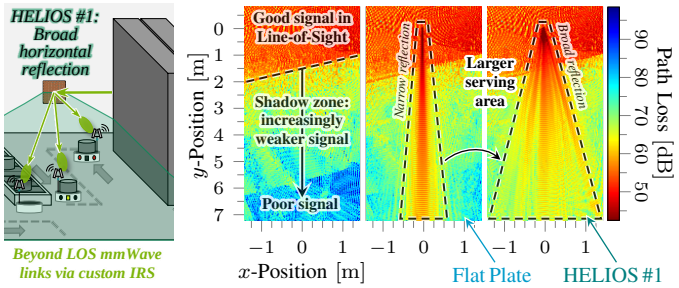

(a) AGVs in area served by broad horizontal reflection at fixed height.

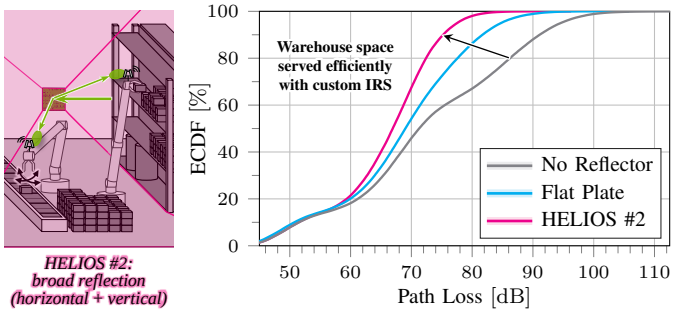

(b) Broad reflection serves storage system robots at various heights.

Fig. 11. Assessing impact of application-tailored IRSs on path loss within a shadowed section of an indoor factory mmWave private network.

the tail is reduced when mounting a reflector, i.e., connectivity is particularly improved in deep shadow regions. Using the custom-designed HELIOS #2 IRS, the 90 % quantile is improved by 15.9 dB and peak gains up to about 30 dB can be observed again. The narrow reflecting surface has a reduced impact, however, gains of more than 10 dB are still observed at a fraction of UE positions in the 3D grid as the reflection is well-aligned to the center of the shadowed volume. Nonetheless, the additional gains for the HELIOS reflector over the narrow-reflecting IRS underline the potential of using the proposed design process to improve connectivity in a predefined region.

V. Conclusions

This manuscript considered HELIOS reflectors constituting a geometry-based approach for scalable IRSs. Motivated by the challenge of efficient mmWave connectivity in indoor factories, an EM simulation-based design approach using differential evolution was proposed. Two distinct IRSs with broad reflections were designed to illuminate a large NLOS region. Our experimental evaluation identified a better reflection behavior than similarly configured reference IRSs by improving the receive power by up to 16 dB over an angular range of more than 20°. These results also indicate that transparent realizations of HELIOS reflectors are feasible. Moreover, our simulative investigation showed that the employed configurations broadly boost mmWave connectivity in the evaluation scenario, particularly in deep shadows with gains of up to about 30 dB. The reduced peak gain of the broad-reflecting IRSs compared to a narrow-reflecting IRS, represented by a flat plate in this work, has little impact compared to the reflection width. Nonetheless, we showed that this can be compensated for by increasing the size of the additive manufactured IRS.

This work further found that the customized reflectors can be used in the entire FR2 spectrum, thereby exhibiting a significantly broader bandwidth than synthetic IRSs. As mmWave cells are co-deployed with a sub-6 GHz anchor cell, we also measured the impact of the designed mmWave reflectors at such frequencies. There, the geometry is relatively flat compared to the wavelength so that the reflection is similar to that of a flat plate. A link budget gain of approximately 10 dB is observed which, as a positive side-effect of the mmWave IRS, allows for higher energy efficiency in the anchor link.

The reflecting surfaces designed in this work have been transferred into a real mmWave deployment and validated from higher-layer perspective using commercial modems [3]. In our future works, we will deploy the HELIOS reflectors in large-scale scenarios for which a faster configuration process shall be adopted using a novel analytical reflection model.

Acknowledgment

This work has been funded by the German Federal Ministry of Education and Research (BMBF) in the course of the *6GEM Research Hub* under grant no. 16KISK038 and the *6G-ANNA* project under grant no. 16KISK101, and by the Ministry of Economic Affairs, Industry, Climate Action, and Energy of the State of North Rhine-Westphalia (MWIKE NRW) along with the *Competence Center 5G.NRW* under grant no. 005-01903-0047.

References

[1] M. Di Renzo *et al.*, "Smart radio environments empowered by reconfigurable intelligent surfaces: How it works, state of research, and the road ahead," *IEEE J. Sel. Areas Commun.*, vol. 38, no. 11, Nov. 2020.

[2] J. Huang *et al.*, "Reconfigurable intelligent surfaces: Channel characterization and modeling," *Proc. IEEE*, vol. 110, no. 9, Sep. 2022.

[3] M. Danger, S. Häger, K. Heimann, S. Böcker, and C. Wietfeld, "Empowering 6G industrial indoor networks: Hands-on evaluation of IRS-enabled multi-user mmWave connectivity," in *Proc. EuCNC/6G Summit*, Jun. 2024.

[4] E. Martinez-de-Rioja *et al.*, "Enhancement of 5G millimeter-wave coverage in indoor scenarios by passive shaped-beam reflectarray panels," in *Proc. EuCAP*, Mar. 2022.

[5] TMY Technology Inc. Passive RIS for fixed-beam redirection.

[6] J. S. Romero-Peña and N. Cardona, "Irregular multifocal reflector for efficient mmWave propagation in indoor enviroments," in *Proc. EuCAP*, Mar. 2020.

[7] X. Liu *et al.*, "Terahertz beam steering using a MEMS-based reflectarray configured by a genetic algorithm," *IEEE Access*, vol. 10, Aug. 2022.

[8] K. Qian *et al.*, "MilliMirror: 3D printed reflecting surface for millimeter-wave coverage expansion," in *Proc. ACM MobiCom*, Oct. 2022.

[9] S. Häger, K. Heimann, S. Böcker, and C. Wietfeld, "Holistic enlightening of blackspots with passive tailorable reflecting surfaces for efficient urban mmWave networks," *IEEE Access*, vol. 11, Apr. 2023.

[10] K. Heimann, S. Häger, and C. Wietfeld, "Demo abstract: Experimental 6G research platform for digital twin-enabled beam management," in *Proc. ACM MobiWac*, Oct. 2023, video: https://tiny.cc/HeliosDemonstrator.

[11] A. P. Ganesh *et al.*, "Propagation measurements and coverage analysis for mmWave and sub-THz frequency bands with transparent reflectors," in *Proc. IEEE VTC-Spring*, Jun. 2023.

[12] N. A. Abbasi *et al.*, "Ultra-wideband double directional channel measurements for THz communications in urban environments," in *Proc. IEEE ICC*, Jun. 2021.

[13] C. K. Anjinappa, F. Erden, and I. Güvenc, "Base station and passive reflectors placement for urban mmWave networks," *IEEE Trans. Veh. Technol.*, vol. 70, no. 4, Apr. 2021.

[14] G. Oliveri *et al.*, "Constrained design of passive static EM skins," *IEEE Trans. Antennas Propag.*, vol. 71, no. 2, Feb. 2023.

[15] U. Mehboob *et al.*, "Genetic algorithms in wireless networking: Techniques, applications, and issues," *Springer Soft Computing J.*, vol. 20, Feb. 2016.

[16] M. Al Hajj *et al.*, "On beam widening for RIS-assisted communications using genetic algorithms," in *Proc. EuCNC/6G Summit*, Jul. 2023.

[17] W. Khawaja *et al.*, "Coverage enhancement for NLOS mmWave links using passive reflectors," *IEEE Open J. Commun. Soc. (OJ-COMS)*, vol. 1, Jan. 2020.

[18] H. Schippers and C. Wietfeld, "Data-driven energy profiling for resource-efficient 5G vertical services," in *Proc. IEEE CCNC*, Jan. 2024.